


***Ab initio* guided minimal model for the “Kitaev” material BaCo<sub>2</sub>(AsO<sub>4</sub>)<sub>2</sub>: Importance of direct hopping, third-neighbor exchange, and quantum fluctuations**Pavel A. Maksimov<sup>1,2</sup>, Alexey V. Ushakov,<sup>2</sup> Zlata V. Pchelkina<sup>1,2,3</sup>, Ying Li,<sup>4</sup>  
Stephen M. Winter,<sup>5</sup> and Sergey V. Streltsov<sup>2,3,\*</sup><sup>1</sup>*Bogolyubov Laboratory of Theoretical Physics, Joint Institute for Nuclear Research, Dubna, Moscow Region 141980, Russia*<sup>2</sup>*M. N. Miheev Institute of Metal Physics, Ural Branch of Russian Academy of Sciences, S. Kovalevskaya Street 18, 620990 Ekaterinburg, Russia*<sup>3</sup>*Department of Theoretical Physics and Applied Mathematics, Ural Federal University, Mira Street 19, 620002 Ekaterinburg, Russia*<sup>4</sup>*Department of Applied Physics and MOE Key Laboratory for Nonequilibrium Synthesis and Modulation of Condensed Matter, School of Physics, Xi’an Jiaotong University, Xi’an 710049, China*<sup>5</sup>*Department of Physics and Center for Functional Materials, Wake Forest University, North Carolina 27109, USA* (Received 20 April 2022; revised 21 September 2022; accepted 13 October 2022; published 31 October 2022)

By considering two *ab initio*-based complementary approaches, we analyze the electronic structure and extract effective spin models of BaCo<sub>2</sub>(AsO<sub>4</sub>)<sub>2</sub>, a honeycomb material which has been proposed as a candidate for Kitaev physics. Both methods show that the dominant direct hopping makes the bond-dependent Kitaev term negligible, diverting the material away from the sought-after spin-liquid regime. As a result, we present a simple three-parameter exchange model to describe the interactions of the lowest doublet of the honeycomb cobaltate BaCo<sub>2</sub>(AsO<sub>4</sub>)<sub>2</sub>. Remarkably, it is the third-neighbor interactions, both isotropic and anisotropic, that are responsible for the standout double-zigzag ground state of BaCo<sub>2</sub>(AsO<sub>4</sub>)<sub>2</sub>, stabilized by quantum fluctuations. A significantly large third-nearest-neighbor hopping, observed *ab initio*, supports the importance of the third-neighbor interactions in the stabilization of the unique ground state of BaCo<sub>2</sub>(AsO<sub>4</sub>)<sub>2</sub>.

DOI: [10.1103/PhysRevB.106.165131](https://doi.org/10.1103/PhysRevB.106.165131)**I. INTRODUCTION**

In the search for material realizations of Kitaev quantum spin liquids [1], a whole family of honeycomb cobaltates, including BaCo<sub>2</sub>(AsO<sub>4</sub>)<sub>2</sub>, BaCo<sub>2</sub>(PO<sub>4</sub>)<sub>2</sub>, CoTiO<sub>3</sub>, and many others [2–20], was proposed to host dominant nearest-neighbor Kitaev exchange couplings, following the concept that Co<sup>2+</sup> ions (3d<sup>7</sup>) in an octahedral crystal field environment with total spin  $S = 3/2$  and orbital angular momentum  $l_{\text{eff}} = 1$  build spin-orbit coupled  $j_{\text{eff}} = 1/2$  doublet states. However, this proposal was recently put into question by a combination of first-principles-based calculations with single-site exact diagonalization and two-site perturbation theory [21]; it was found that the Kitaev term favoring a spin-liquid ground state must be rather small.

In the present work we perform a detailed analysis of the electronic structure within density functional theory (DFT) employing the projector augmented-wave [22] basis as implemented in VASP, as well as the full potential local orbital (FPLO) basis [23]. We further use two *ab initio*-based complementary approaches to extract effective spin models for the honeycomb cobaltate BaCo<sub>2</sub>(AsO<sub>4</sub>)<sub>2</sub>. One is based on total energy calculations of various magnetic configurations within DFT +  $U$  + spin-orbit coupling (SOC) and mapping into a spin model to extract the exchange tensor elements, and the second method is based on the projED method [24,25]

recently introduced by some of the authors, which consists of a combination of DFT calculations, exact diagonalization (ED) of extracted generalized relativistic Hubbard models on finite clusters, and projection to low-energy spin Hamiltonians. We find that the Kitaev model is hardly applicable for a description of the magnetic properties of BaCo<sub>2</sub>(AsO<sub>4</sub>)<sub>2</sub>, which is supported by both *ab initio* calculations and the phenomenology of BaCo<sub>2</sub>(AsO<sub>4</sub>)<sub>2</sub>.

One of the peculiarities of BaCo<sub>2</sub>(AsO<sub>4</sub>)<sub>2</sub> is the long search for the correct magnetic ground state. Early works suggested that the ground state is an unusual long-range ordered spiral state with in-plane ordering vector  $\mathbf{Q} = (0, \pi/3)$  [13]. However, more refined neutron scattering data later showed that the ground state is instead a collinear double-zigzag state [15] with the  $++--$  pattern of zigzag chains with the magnetic moments approximately parallel to the chain direction. Since the model including isotropic exchange between the nearest and third-nearest neighbors ( $J_1$ - $J_3$  model) does not reproduce this experimentally established magnetic order, the Hamiltonian requires extra terms beyond the isotropic third-neighbor interaction in order to describe the ground state of BaCo<sub>2</sub>(AsO<sub>4</sub>)<sub>2</sub>. Indeed, *ab initio* studies in this work and in earlier works [21] indicate a significant role of anisotropic couplings associated with the spin-orbital  $j_{\text{eff}} = 1/2$  moments of 3d<sup>7</sup> Co<sup>2+</sup>. This is further supported by the finite-energy gap observed in inelastic neutron scattering data and terahertz spectroscopy, although the small magnitude of this gap ( $\sim 1.45$  meV [15]) places constraints on the magnitude of anisotropic terms.

\*streltsov@imp.uran.ru

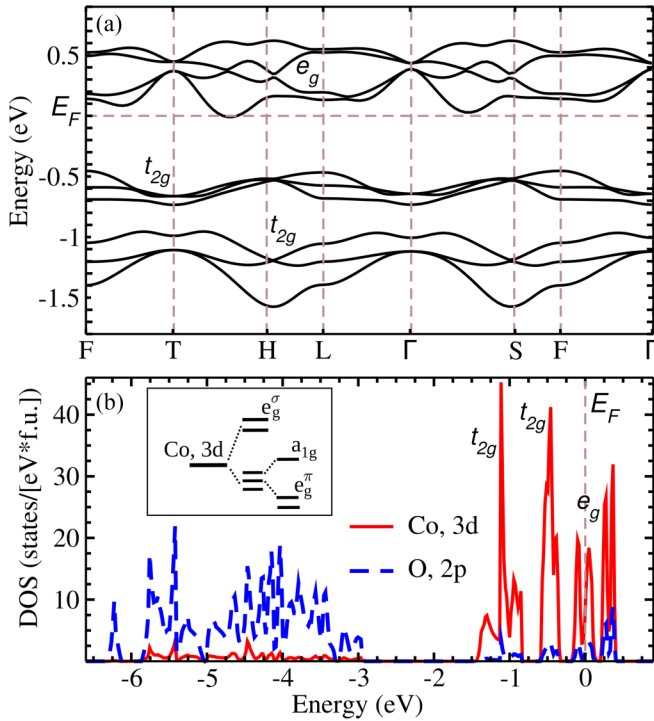


FIG. 1. (a) The band structure and (b) partial densities of states of  $\text{BaCo}_2(\text{AsO}_4)_2$  at the GGA level.

In this paper we extensively study the phase diagram of the general eight-parameter model to identify which exchange parameters are essential in the stabilization of the double-zigzag state. We find that it is the third-neighbor isotropic and anisotropic terms that are crucial and make up a minimal model required to describe the magnetic properties of  $\text{BaCo}_2(\text{AsO}_4)_2$ . Even though the *ab initio* parameter sets yield the zigzag ground state, they are close to the phase boundary. Therefore, we argue that there can be additional corrections, such as magnetoelastic coupling, which can tune the calculation towards the experimentally observed double-zigzag ground state.

## II. DFT: CRYSTAL-FIELD AND HOPPING PARAMETERS

We start with the analysis of the on-site Hamiltonian obtained in nonmagnetic DFT using both maximally localized Wannier functions [26] within VASP [27] and FPLO [23,28] basis sets. All calculation details are given in the Supplemental Material (SM) [29] (see also Refs. [30–41] therein).

The crystal structure of  $\text{BaCo}_2(\text{AsO}_4)_2$  is characterized by the  $R\bar{3}$  space group. It consists of stacked honeycomb layers of edge-sharing  $\text{CoO}_6$  octahedra along the  $c$  axis separated by bilayers of opposite-facing  $\text{AsO}_4$  tetrahedra with Ba atoms in between. The cubic crystal field of the  $\text{O}_6$  octahedron around Co splits the Co 3d orbitals into  $e_g^\sigma$  and  $t_{2g}$  states, and the latter are then further split by additional trigonal distortions into lower-lying  $e_g^\pi$  and  $a_{1g}$  states because of the layered structure [see the inset in Fig. 1(b)]. In Ref. [21], these splittings were estimated by rescaling values (to fit available experimental data) obtained from  $N$ th muffin-tin orbital calculations, leading to 735 meV for the  $e_g^\sigma$ - $a_{1g}$  splitting and to 94 meV for

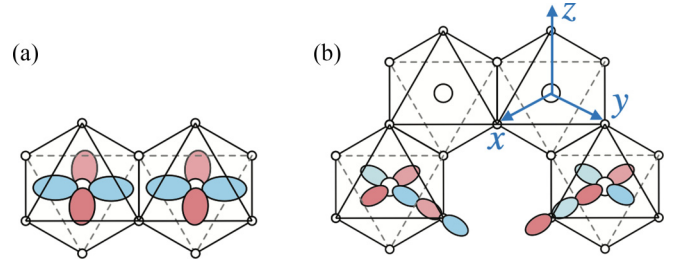


FIG. 2. Sketch illustrating two dominating hopping processes according to DFT calculations. (a) Direct nearest-neighbor overlap of two  $xy$  orbitals. (b) Largest contributions for third-nearest neighbors corresponding to hoppings between  $x^2-y^2$  orbitals via O  $2p$  states.

the splitting within  $t_{2g}$  ( $a_{1g}$ - $e_g^\pi$ ). Our DFT (VASP) calculations give similar results, 818 and 122 meV, respectively, without any additional renormalization. Interestingly, with the FPLO basis, Wannier projection [36] leads to somewhat larger values of 963 and 133 meV. However, it should be emphasized that in all cases the latter  $t_{2g}$  splitting is comparable to the atomic spin-orbit coupling constant  $\lambda_{\text{Co}} \approx 60$  meV defined by  $\mathcal{H}_{\text{SOC}} = \lambda \mathbf{S} \cdot \mathbf{L}$ , suggesting strong deviations from ideal  $j_{\text{eff}} = 1/2$  moments at the Co sites. This finding is also consistent with the strong reported anisotropy of the  $g$  tensor ( $g_{ab} \sim 2g_c$ ) [15].

We utilized several approaches for the nearest-neighbor hopping integrals: Wannier function projection [26], projected localized orbitals [35] as implemented in VASP, and FPLO [36]. Notably, all approaches we used led to the same conclusions. For instance, for the bond depicted in Fig. 2(a), the direct  $xy/xy$  hopping  $t' \sim -300$  meV dominates over hoppings via  $xz$  and  $yz$  orbitals,  $t \sim 50$  meV, which are associated with electron transfer via ligand  $p$  states; the local coordinate system shown in Fig. 2(b) is chosen. Similar findings were recently reported for  $\text{Na}_2\text{BaCo}(\text{PO}_4)_2$  [42] and other edge-sharing Co compounds [43]. Already, this fact reveals that one of the key assumptions used in [2],  $\kappa = |t'/t| < 1$ , is far from being fulfilled. This results in a small Kitaev exchange for the first-nearest neighbors, as we will demonstrate in the next section. It is worth mentioning that a large  $xy/xy$  hopping not only affects exchange coupling but also strongly changes the electronic structure. One can clearly observe the formation of two isolated branches of Co  $t_{2g}$  bands in Fig. 1, where each of the  $t_{2g}$  orbitals has a direct overlap with the corresponding orbital on one of the neighboring Co sites. Indeed, the gap between these bands closes if the direct  $xy/xy$  hopping is set to zero, as explained in the SM.

Another very important feature, which becomes evident already on the DFT level, is that hopping between third-nearest neighbors  $t_3$  is not small. The most important contribution comes from hopping between  $e_g$  orbitals, which strongly hybridize with ligand  $p$  orbitals. This leads, for example, to an effective hopping  $t_3^{x^2-y^2/x^2-y^2} \approx 124$  meV [see Fig. 2(b)]. This hopping is associated with an antiferromagnetic  $J_3$  that may be comparable to the nearest-neighbor exchange  $J_1$ . This finding contradicts the assumption [2,3,44] that longer-range couplings should be suppressed in  $3d^7$  compounds as a result of stronger Coulomb interactions and smaller  $d$  orbitals localizing the moments in comparison to traditional  $4d^5$  and  $5d^5$

Kitaev candidate materials. In fact, the partial filling of the  $e_g$  orbitals in  $3d^7$   $\text{Co}^{2+}$  provides additional long-range exchange pathways. Large hopping between the third-nearest neighbors is also reflected in the electronic structure of  $\text{BaCo}_2(\text{AsO}_4)_2$ . It results in the formation of the bonding and antibonding  $e_g$  states, as discussed in the SM, which is clearly seen in Fig. 1.

### III. AB INITIO EXCHANGE PARAMETERS

Due to the interplay of crystal field and SOC, the magnetic interactions of effective doublets are defined by the symmetry of the lattice. The symmetry of edge-sharing  $\text{CoO}_6$  octahedra results in the extended Kitaev-Heisenberg model [45], which has been discussed for  $\text{BaCo}_2(\text{AsO}_4)_2$  [3]. Explicitly, the exchange Hamiltonian is given by

$$\hat{\mathcal{H}}_{\text{cubic}} = \sum_{(ij)_n} J_n \mathbf{S}_i \cdot \mathbf{S}_j + K_n S_i^\gamma S_j^\gamma + \Gamma_n (S_i^\alpha S_j^\beta + S_i^\beta S_j^\alpha) + \Gamma'_n (S_i^\gamma S_j^\alpha + S_i^\alpha S_j^\gamma + S_i^\beta S_j^\gamma + S_i^\gamma S_j^\beta), \quad (1)$$

where the sum is taken over the three types of bonds of the honeycomb lattice,  $\{\alpha, \beta, \gamma\} = \{x, y, z\}$  for the  $Z$ -type bond and interactions on the  $X$  and  $Y$  bonds are obtained through a cyclic permutation [45,46] [see Fig. 3(a)]. Note that this model uses cubic axes  $\{x, y, z\}$ , which are shown in Figs. 2 and 3(a) and are related to the ion-ligand bonds. In accordance with neutron studies and *ab initio* results below, we anticipate that first-neighbor ( $n = 1$ ) and third-neighbor ( $n = 3$ ) couplings are dominant.

For our purpose, it is also convenient to refer the interactions alternatively to the crystallographic axes  $\{x, y, z\}$ , which are defined by the honeycomb plane of magnetic ions, shown in Fig. 3(a). The Hamiltonian in that reference frame is given by

$$\hat{\mathcal{H}}_{\text{cryst}} = \sum_{(ij)_n} J_n (S_i^x S_j^x + S_i^y S_j^y + \Delta_n S_i^z S_j^z) - 2J_{\pm\pm}^{(n)} [(S_i^x S_j^x - S_i^y S_j^y) c_\alpha - (S_i^x S_j^y + S_i^y S_j^x) s_\alpha] - J_{z\pm}^{(n)} [(S_i^x S_j^z + S_i^z S_j^x) c_\alpha + (S_i^y S_j^z + S_i^z S_j^y) s_\alpha], \quad (2)$$

where  $c_\alpha \equiv \cos \varphi_\alpha$  and  $s_\alpha \equiv \sin \varphi_\alpha$  with the bond-dependent phases  $\varphi_\alpha = \{0, 2\pi/3, -2\pi/3\}$  for the three types of first- and third-neighbor bonds [45,47]. The exchange parameters of the extended Kitaev-Heisenberg model (1) and anisotropic-exchange model in the crystallographic axes (2) are related through a simple linear transformation:

$$\begin{aligned} J_n &= \frac{1}{3}(2J_n + \Delta_n J_n + 2J_{\pm\pm}^{(n)} - \sqrt{2}J_{z\pm}^{(n)}), \\ K_n &= -2J_{\pm\pm}^{(n)} + \sqrt{2}J_{z\pm}^{(n)}, \\ \Gamma_n &= \frac{1}{3}(-J_n + \Delta_n J_n - 4J_{\pm\pm}^{(n)} - \sqrt{2}J_{z\pm}^{(n)}), \\ \Gamma'_n &= \frac{1}{6}(-2J_n + 2\Delta_n J_n + 4J_{\pm\pm}^{(n)} + \sqrt{2}J_{z\pm}^{(n)}). \end{aligned} \quad (3)$$

We use a variety of approaches to estimate the magnetic exchange couplings. Conventional DFT calculations underestimate the effect of strong Coulomb correlations, which must be taken into account for extraction of the exchange interaction in transition metal oxides. We therefore first computed the magnetic interactions based on a DFT(GGA)+ $U$ +SOC

TABLE I. The dependence of exchange interaction parameters on on-site Coulomb  $U$  computed from DFT+SOC+ $U$  total energy in the extended Kitaev model. Intra-atomic Hund's exchange was chosen to be  $J_H = 0.9$  eV.

	$U$		
	5 eV	6 eV	7 eV
$J_1$ (K)	-61.0	-40.9	-37.6
$K_1$ (K)	0.3	2.2	5.3
$\Gamma_1$ (K)	-2.2	-1.7	-1.8
$\Gamma'_1$ (K)	5.1	4.0	3.2
$J_3$ (K)	31.4	24.6	18.7
$K_3$ (K)	-0.2	0.2	-0.2
$\Gamma_3$ (K)	-4.5	-6.0	-4.5
$\Gamma'_3$ (K)	-3.6	-2.3	-1.8

calculation of total energies of four noncolinear magnetic configurations [41], where GGA is the generalized gradient approximation. These results are complemented by extraction of the couplings from exact diagonalization of two-site clusters, which are described below.

For the total energy DFT(GGA)+ $U$ +SOC calculations, the most important exchanges for the first- and third-nearest neighbors are summarized in Tables I and II in terms of both extended Kitaev and crystallographic parametrizations (other constants were found to be small, e.g.,  $J_2 \sim 0.2$  K). The calculations were performed for several values of the on-site Hubbard repulsion parameter  $U$ , but all of them demonstrate that (i) the Kitaev exchange is small for both the first- and third-nearest neighbors and that (ii) there is a strong exchange coupling with third-nearest neighbors. Both factors strongly suppress formation of a spin-liquid state and are compatible with a previous neutron scattering analysis, which suggested  $J_1 \sim -38$  K and  $J_3 \sim +10$  K [14], as well as more recent data [48], which estimated  $J_1 \sim -88$  K,  $J_3 \sim +29$  K, and  $J_{\pm\pm}^{(1)} \sim -0.6$  K. We note, however, that large  $XXZ$  anisotropy estimated from experiment ( $\Delta \sim 0.37$  [14] and  $\Delta_1 \sim 0.16$  [48]) is not reproduced in this approach.

TABLE II. The dependence of exchange interaction parameters on on-site Coulomb  $U$  in the crystallographic parametrization. Intra-atomic Hund's exchange was chosen to be  $J_H = 0.9$  eV.

	$U$		
	5 eV	6 eV	7 eV
$J_1$ (K)	-63.6	-42.3	-37.4
$\Delta_1$	0.87	0.85	0.88
$J_{\pm\pm}^{(1)}$ (K)	2.4	1.5	0.8
$J_{z\pm}^{(1)}$ (K)	3.5	3.7	4.9
$J_3$ (K)	35.2	28.2	21.3
$\Delta_3$	0.67	0.62	0.62
$J_{\pm\pm}^{(3)}$ (K)	0.3	1.2	0.9
$J_{z\pm}^{(3)}$ (K)	0.3	1.8	1.2

TABLE III. Exchange interaction parameters (in K) computed from exact diagonalization of the effective  $d$ -orbital model. Values in parentheses include estimated corrections for omitted ligand exchange processes.

	$J_{H,t_{2g}}$			
	0.7 eV		0.9 eV	
	$U = 3.25$ eV	$U = 5$ eV	$U = 6$ eV	$U = 7$ eV
$J_1$ (K)	-107 (-127)	-37 (-57)	-18 (-38)	-8.8 (-29)
$K_1$ (K)	32	13	6.5	3.4
$\Gamma_1$ (K)	28 (35)	14 (21)	8.0 (15)	4.8 (12)
$\Gamma'_1$ (K)	9.4 (16)	7 (14)	4.0 (11)	2.4 (9)
$J_3$ (K)	43	30	27	24
$K_3$ (K)	-0.6	-0.4	-0.3	-0.3
$\Gamma_3$ (K)	-20	-12	-10	-8.9
$\Gamma'_3$ (K)	-21	-12	-11	-9.2

In order to further examine the magnetic couplings, we employed a complementary approach similar to that in Ref. [21]: exact diagonalization of the five- $d$ -orbital model on two sites [24,25]. For this purpose, we employ hopping integrals obtained from VASP and take the fully spherically symmetric form [49] of the on-site Coulomb interactions with Slater parameters  $F_4/F_2 = 0.625$ ,  $F_0 \equiv U$  and  $F_2 \equiv 14J/(1 + 0.625)$  set according to  $U = 5$  to 7 eV, and  $J_{H,t_{2g}} = 0.9$  eV. The results are shown in Table III. For the purpose of comparison, results for Coulomb parameters equivalent to those in Ref. [21] ( $U = 3.25$  eV,  $J_{H,t_{2g}} = 0.7$  eV) are also shown. We note that this approach neglects an important contribution to the exchange involving multiple holes on a given ligand, which can be corrected using expressions from perturbation theory [3,43,50]. This leads to shifts of the nearest-neighbor couplings  $J_1 \rightarrow J_1 + \delta J$ ,  $\Gamma_1 \rightarrow \Gamma_1 + \delta \Gamma$ , and  $\Gamma'_1 \rightarrow \Gamma'_1 + \delta \Gamma$  that can be estimated from the trigonal crystal field splitting and realistic metal-ligand hopping parameters (see [3,43]). In this case, a rough estimate is  $\delta J \sim -20$  K and  $\delta \Gamma \sim +7$  K. Both corrected and uncorrected results are given in Tables III and IV.

The ED + perturbation theory results are essentially compatible with the DFT results above; ferromagnetic  $J_1$  dominates the couplings, while the anisotropic couplings  $K_1$ ,  $\Gamma_1$ ,  $\Gamma'_1 > 0$  are all of smaller but similar magnitude. The main difference is that the  $XXZ$  anisotropy is considerably stronger in ED results, with corrected values of  $\Delta_1$  ranging between 0.2 and 0.5. This anisotropy originates from the effects of local trigonal crystal field on the  $j_{\text{eff}} = 1/2$  multiplet structure, which may not be completely captured in one-electron methods such as DFT+ $U$ +SOC. On the other hand, cluster approaches, such as our ED method, tend to have difficulties with long-range interactions. This fact is embodied by surprisingly large  $J_3$ , which is comparable to  $J_1$ , as can be seen in Table IV.

Thus, both calculation methods rather guide than provide exact estimates of exchange constants. It is important that our methods and the perturbation theory of Ref. [21] give consistent results, which is not always the case for Kitaev materials (for  $\text{Li}_2\text{IrO}_3$  see Refs. [25,51], and for  $\alpha\text{-RuCl}_3$  see

TABLE IV. Exchange interaction parameters computed from exact diagonalization of the effective  $d$ -orbital model. Values in parentheses include estimated corrections for omitted ligand exchange processes.

	$J_{H,t_{2g}}$			
	0.7 eV		0.9 eV	
	$U = 3.25$ eV	$U = 5$ eV	$U = 6$ eV	$U = 7$ eV
$J_1$ (K)	-113 (-140)	-42 (-69)	-21 (-48)	-11 (-38)
$\Delta_1$	0.58 (0.51)	0.36 (0.31)	0.24 (0.23)	0.11 (0.19)
$J_{\pm\pm}^{(1)}$ (K)	-12	-4.5	-2.4	-1.4
$J_{z\pm}^{(1)}$ (K)	6.2	2.7	1.2	0.4
$J_3$ (K)	64	42	37	33
$\Delta_3$	$\sim 0$	0.14	0.16	0.18
$J_{\pm\pm}^{(3)}$ (K)	0.1	$\sim 0$	$\sim 0$	$\sim 0$
$J_{z\pm}^{(3)}$ (K)	-0.60	-0.36	-0.30	-0.26

Ref. [52]). However, both approaches place the system in a region of zigzag order for all of the presented parameter sets, rather than the double-zigzag observed in  $\text{BaCo}_2(\text{AsO}_4)_2$ . In the next section we show that these parameter sets are, in fact, close to the boundary of the double-zigzag phase, and extensively study the full phase diagram in order to establish which of the parameters of the model would tune the ground state towards the experimentally established one.

#### IV. PHASE DIAGRAM

We now investigate the minimal set of interactions that is compatible with the ground state phenomenology of  $\text{BaCo}_2(\text{AsO}_4)_2$  [16]. We start with the isotropic  $XY$   $J_1$ - $J_3$  model, guided by *ab initio* sets presented above, and study phase transitions when the anisotropic-exchange terms of the full eight-parameter model (2) are added to the Hamiltonian one at a time, using the classical Luttinger-Tisza (LT) method [53]. We should note that in frustrated magnets with broken continuous symmetry, incommensurate spiral states given by Luttinger-Tisza approach cannot satisfy local spin constraints and thus are not exact classical ground states [54]. However, even though the LT method breaks down, it can still point to regions of exotic ground states on the phase diagram [46,55,56]. Therefore, we use the LT method in this section as a guide for the search of classical ground states beyond ferromagnetic and zigzag phases by plotting the ordering vector selected by LT, and we take the boundary of stability of the LT method as an indicator of the regions of the phase diagram which can host the double-zigzag state (which is studied in detail in the next section).

Corresponding phase diagrams are shown in Fig. 3, where we plot the ordering vector  $(0, Q_y)$  as an intensity map, and the regions where the LT method breaks down are shown by white dashed lines. As depicted in the Brillouin zone in Fig. 3(b),  $Q_y = 0$  corresponds to a ferromagnetic (FM) state,  $Q_y = 2\pi/3$  corresponds to a zigzag state, and the spiral state originally proposed for  $\text{BaCo}_2(\text{AsO}_4)_2$  interpolates between these states with  $0 < Q_y < 2\pi/3$ . The  $J_1$ - $J_3$  model is known

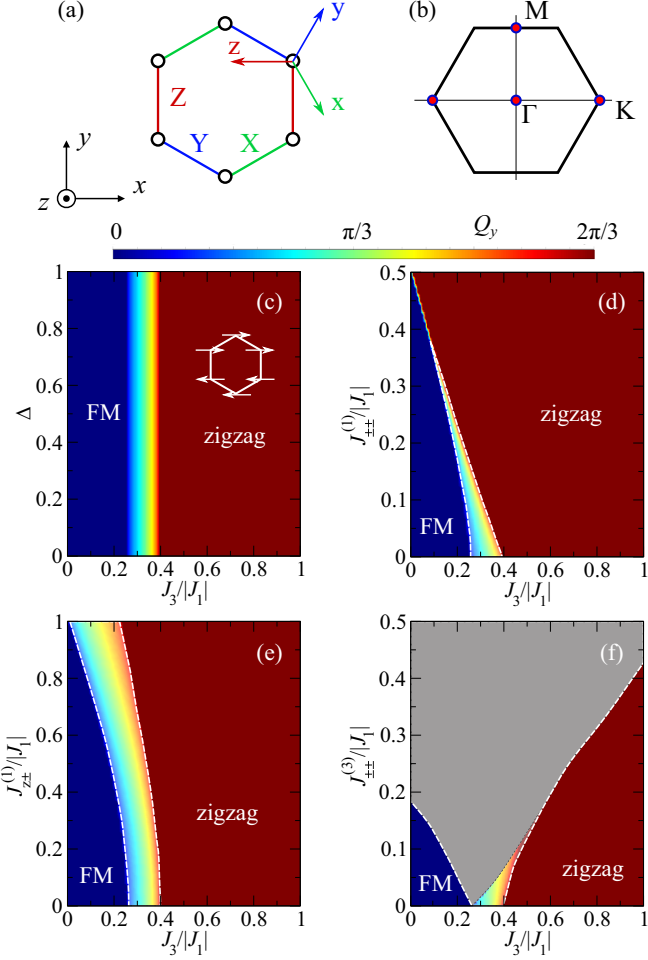


FIG. 3. (a) Honeycomb lattice with three types of bonds; cubic axes  $\{x, y, z\}$  and crystallographic axes  $\{x, y, z\}$  are also presented. (b) Brillouin zone of the honeycomb lattice with high-symmetry points indicated. (c)–(f) Classical phase diagram of the model (2) calculated with the Luttinger-Tisza method for  $J_1 < 0$ ,  $J_3 > 0$ ,  $\Delta = \Delta_1 = \Delta_3$ . The ordering vector of the classical spiral state  $Q_y$  is represented by the color intensity map. A sketch of the zigzag is shown as an inset. The state shown with gray has a non-zero  $Q_x$  component of the ordering vector and thus is not related to the ground state of  $\text{BaCo}_2(\text{AsO}_4)_2$ .

to host this spiral state for  $0.25|J_1| < J_3 < 0.4|J_1|$  [57], as shown in Fig. 3(c), and the addition of XXZ anisotropy (with  $\Delta = \Delta_1 = \Delta_3$ ) does not alter the relative stabilities of the phases compared to the pure Heisenberg  $J_1$ - $J_3$  model.

In contrast, the addition of anisotropic first-neighbor  $J_{\pm\pm}^{(1)}$  and  $J_{z\pm}^{(1)}$  exchange terms stabilizes the zigzag state [see Figs. 3(d) and 3(e)]. However, the  $J_{\pm\pm}^{(3)}$  interaction promotes non-FM and nonzigzag states, shown in gray in Fig. 3(f). However, LT suggests states with the ordering vector near the  $K$  point with a nonzero  $Q_x$  component; thus, this region is not relevant to the ground state of  $\text{BaCo}_2(\text{AsO}_4)_2$ , and we do not go into the specifics of its structure.

Finally, we also considered phase diagrams starting from the DFT and ED parameters. For this purpose, we use the results for  $U = 5$  eV in each case, as the corresponding inter-

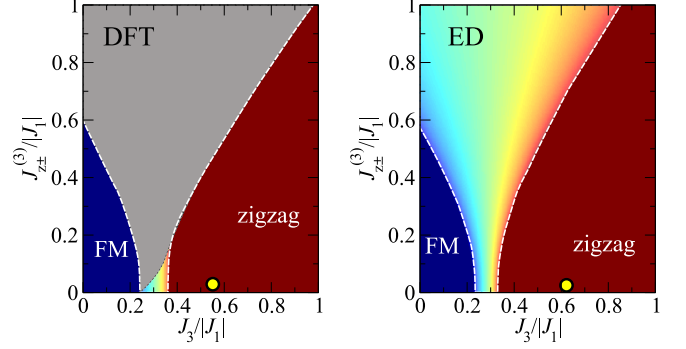


FIG. 4. Luttinger-Tisza  $J_3$ - $J_{z\pm\pm}^{(3)}$  phase diagrams for  $U = 5$  eV sets of parameters from Tables I and III. DFT and ED parameter sets are indicated with yellow dots.

actions are closest in magnitude to the experimental estimates [14,48]. Results are shown in Fig. 4 with respect to tuning  $J_3$  and  $J_{z\pm\pm}^{(3)}$ . The latter third-neighbor interaction was selected because it tends to stabilize the  $(0, Q_y)$  spiral when added to the both the isotropic  $J_1$ - $J_3$  and ED models. As can be seen, both *ab initio* parameter sets predict the zigzag as a ground state, but both lie relatively close to the boundary of the zigzag state. While we find that various modifications of these parameters may stabilize the spiral phase (such as increasing  $J_{z\pm\pm}^{(3)}$  with respect to the ED couplings), the discrepancy is most likely attributable to an overestimation of third-neighbor couplings. That is, rescaling of  $J_3$  shifts both parameter sets towards the spiral state. As we show in the next section, the spiral is, indeed, replaced by the unique double-zigzag state in a more careful study of the classical ground state and when quantum fluctuations are taken into consideration.

## V. DOUBLE-ZIGZAG STATE

In order to search for the double-zigzag state and explore quantum effects on the relevant phases, we focus on a reduced three-parameter  $J_1$ - $J_3$ - $J_{z\pm\pm}^{(3)}$  model as a minimal Hamiltonian for  $\text{BaCo}_2(\text{AsO}_4)_2$ :

$$\hat{\mathcal{H}}_{\min} = \sum_{\langle ij \rangle_1} J_1 (S_i^x S_j^x + S_i^y S_j^y) + J_3 \sum_{\langle ij \rangle_3} (S_i^x S_j^x + S_i^y S_j^y) - J_{z\pm\pm}^{(3)} [(S_i^x S_j^z + S_i^z S_j^x) c_\alpha + (S_i^y S_j^z + S_i^z S_j^y) s_\alpha]. \quad (4)$$

We take easy-plane anisotropy  $\Delta_1 = \Delta_3 = 0$ . This choice of minimal interactions is sufficient to provide a wide region of stability for the double-zigzag phase, although it neglects many interactions relevant to the real material.

First, the LT phase diagram of the model (4) presented in Fig. 5(a) points to a state with the  $(0, Q_y)$  ordering vector. However, since the incommensurate spiral state given by LT does not satisfy the strong local spin length constraint, we perform a more focused study of the classical ground state. We use a quasi-one-dimensional cluster, periodic in the  $x$  axis, using the fact that spin modulation is only along the  $y$  axis, as suggested by the  $(0, Q_y)$ -spiral state from LT calculations. The results of classical energy minimization on a 24-unit cell cluster are shown in Fig. 5(b), where the color intensity illustrates the magnitude of the  $Q_y$  ordering vector. We can see

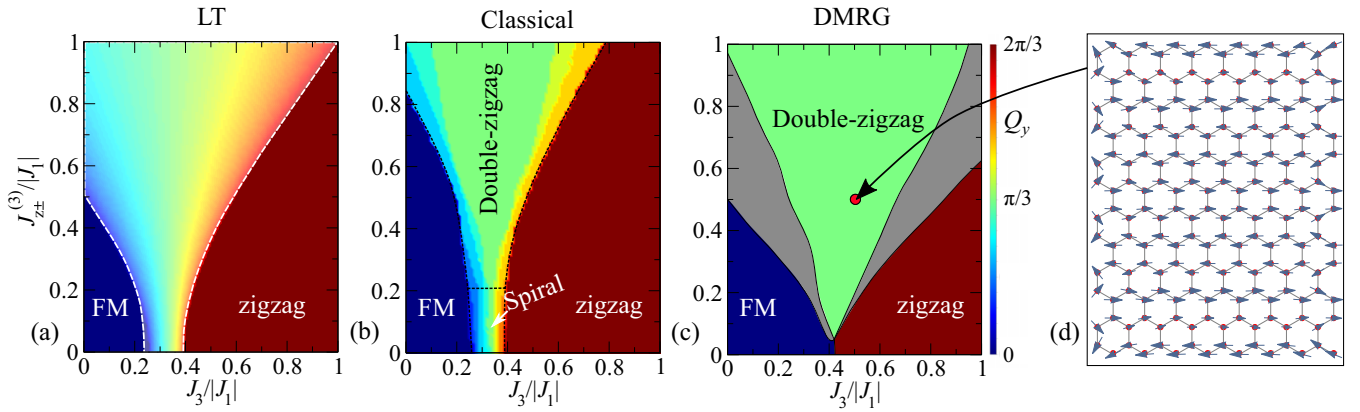


FIG. 5. (a) Luttinger-Tisza phase diagram of the XY (i.e.,  $\Delta = 0$ )  $J_1$ - $J_3$ - $J_{z\pm}^{(3)}$  model (4) calculated with the Luttinger-Tisza method for  $J_1 < 0, J_3 > 0$ . The ordering vector of the classical state  $Q_y$  is represented by the color intensity map. (b) Classical phase diagram of the model (4) with the same notation for the intensity map. (c) DMRG phase diagram of the model (4) for  $S = 1/2$ . The gray areas indicate regions of the intermediate phases which are beyond the scope of this work. (d) Example of the DMRG calculation for a representative parameter set  $J_3 = J_{z\pm}^{(3)} = 0.5|J|$  which exhibits a double-zigzag ground state.

that, compared to the LT method, the double-zigzag state is, in fact, stabilized in the phase diagram of the  $J_1$ - $J_3$ - $J_{z\pm}^{(3)}$  model for  $J_{z\pm}^{(3)} \gtrsim 0.2$ , while the spiral state is stable for  $J_{z\pm}^{(3)} \lesssim 0.2$ .

Moreover, it is known that there are strong renormalizations of phase diagrams of frustrated quantum  $S = 1/2$  models relative to the classical  $S \rightarrow \infty$  approximation [46,58–67]. In order to study the model (4) in the quantum limit in the context of  $j_{\text{eff}} = 1/2$  moments of  $\text{BaCo}_2(\text{AsO}_4)_2$ , we employ the density matrix renormalization group (DMRG) [68] using the ITENSOR library [69] on a 192-site  $S = 1/2$  cluster with open boundary conditions using 20 sweeps with error  $< 10^{-4}$  and a random initial state. (We have also studied clusters of other sizes and with periodic boundary conditions; they all yielded very similar results.) The phases were identified by the maximum value of spin-spin correlator  $\mathcal{S}(\mathbf{k})$  calculated at  $\Gamma, K, M$ , and  $(0, \pi/3)$ , where

$$\mathcal{S}(\mathbf{k}) = \sum_{i,j} \langle \mathbf{S}_i \cdot \mathbf{S}_j \rangle e^{i\mathbf{k}(\mathbf{r}_i - \mathbf{r}_j)}. \quad (5)$$

The phase diagram, obtained with the DMRG in the quantum  $S = 1/2$  limit, is shown in Fig. 5(c). The ordering vector is shown by the color intensity, the same as in Figs. 5(a) and 5(b); the phases in gray are intermediate between FM, double zigzag, and zigzag, but their characterization is beyond the scope of this work. Note that our investigative DMRG calculation is unable to give a conclusive result in the region of multiple-phase competition for  $J_{z\pm}^{(3)} < 0.1|J_1|$ . Nonetheless, we can see that the double-zigzag state is stable in a wider region of the phase diagram for  $S = 1/2$ , relative to classical model predictions. This fact implies that quantum fluctuations play a significant role, which is captured by the DMRG. This mechanism is generic and applies beyond the minimal model. Such fluctuations are known to stabilize collinear orders in frustrated systems, such as the field-induced up-up-down state in the triangular lattice antiferromagnet [70,71], honeycomb  $J_1$ - $J_2$  model [72], and anisotropic-exchange model on a triangular lattice [56,58,73].

An example of the spin orientations obtained with the DMRG for the representative parameter set  $J_3 = J_{z\pm}^{(3)} = 0.5|J|$  is shown in Fig. 5(c). This observed spin structure is precisely the same as that measured in the latest neutron data [15], the  $++--$  double-zigzag structure. Moreover, an out-of-plane canting of the spins around  $5^\circ$  was also reported [15]. We also observe the out-of-plane canting, induced by the anisotropic  $J_{z\pm}^{(3)}$  term, which couples in-plane and out-of-plane spin components. However, the canting in our DMRG calculation not only has opposite signs between chains of opposite directions but also has different signs between the  $A$  and  $B$  sublattices of the honeycomb lattice.

Finally, we remark on an additional mechanism that may stabilize the mysterious double-zigzag structure. Our DFT+ $U$ +SOC calculations ( $U = 6$  eV) show that the zigzag is the ground state magnetic structure with the double zigzag being 1.2 meV/f.u. higher in energy for the experimental crystal structure. However, relaxation of the atomic positions completely changes the situation: the double-zigzag order becomes more stable than the spiral by 0.2 meV/f.u. ( $\approx 1$  K/Co). The task of deciphering the origin of the stabilization of the double-zigzag structure from *ab initio* calculations is extremely complicated due to a tiny total energy difference (corresponding hopping parameters and nearest-neighbor exchange constants can be found in the SM), but one can conclude with certainty that (i) the system is on the border between two magnetic phases and phase separation or the presence of different domains is not excluded and (ii) the magnetoelastic coupling is important in  $\text{BaCo}_2(\text{AsO}_4)_2$  [74].

## VI. CONCLUSIONS

By means of *ab initio* band structure, Luttinger-Tisza, and DMRG calculations we studied the electronic and magnetic properties of  $\text{BaCo}_2(\text{AsO}_4)_2$ , a candidate material for the realization of the celebrated Kitaev model. While previous theoretical results [3] and experimental data [20] suggested a dominant Kitaev interaction, promising proximity to the spin-liquid regime, in this paper we showed that this notion

is not supported by either phenomenology or various *ab initio* methods.

Instead, DFT and ED in this paper establish that large direct exchange due to  $t_{2g}$  orbitals strongly suppresses anisotropic contributions to the exchange interaction between nearest neighbors, in agreement with Ref. [21]. Moreover, there is also substantial coupling with third-nearest neighbors, such that  $J_3 > 0.3|J_1|$ . These two findings together make the formation of a spin-liquid state unfavorable, driving the system towards the long-range ordered state.

However, proposed *ab initio* models do not yield the unique double-zigzag ground state of  $\text{BaCo}_2(\text{AsO}_4)_2$ . Through an extensive search over the eight-parameter phase space we established a minimal model that hosts the double-zigzag state in a wide range of parameters. Remarkably, quantum fluctuations inherent in  $j_{\text{eff}} = 1/2$  magnets strongly affect the ground state of the proposed model and stabilize the double-zigzag magnetic structure previously observed experimentally. We

showed that proposed parameter sets from *ab initio* calculations are near the boundary of the double-zigzag state, and we suggest that magnetoelastic coupling can play a crucial role since the double-zigzag state can be stabilized by optimization of the crystal structure in DFT+ $U$ +SOC calculations.

## ACKNOWLEDGMENTS

We cannot describe the immeasurable gratitude we have for R. Valentí, whose expertise immensely assisted in the launch of this project and whose numerous insightful discussions aided in guiding the paper in a desirable direction. We would like to thank S. Chernyshev and A. Paramekanti for useful discussions and comments. S.V.S. is grateful to B. Cava and I. Solovyev for fruitful communications. We acknowledge support from the Russian Science Foundation via project 20-62-46047.

- 
- [1] A. Kitaev, Anyons in an exactly solved model and beyond, *Ann. Phys. (NY)* **321**, 2 (2006).
- [2] H. Liu and G. Khaliullin, Pseudospin exchange interactions in  $d^7$  cobalt compounds: Possible realization of the Kitaev model, *Phys. Rev. B* **97**, 014407 (2018).
- [3] H. Liu, J. Chaloupka, and G. Khaliullin, Kitaev Spin Liquid in 3d Transition Metal Compounds, *Phys. Rev. Lett.* **125**, 047201 (2020).
- [4] C. Kim, J. Jeong, G. Lin, P. Park, T. Masuda, S. Asai, S. Itoh, H.-S. Kim, H. Zhou, J. Ma, and J.-G. Park, Antiferromagnetic Kitaev interaction in  $J_{\text{eff}} = 1/2$  cobalt honeycomb materials  $\text{Na}_3\text{Co}_2\text{SbO}_6$  and  $\text{Na}_2\text{Co}_2\text{TeO}_6$ , *J. Phys.: Condens. Matter* **34**, 045802 (2022).
- [5] G. Lin *et al.*, Field-induced quantum spin disordered state in spin-1/2 honeycomb magnet  $\text{Na}_2\text{Co}_2\text{TeO}_6$ , *Nat. Commun.* **12**, 5559 (2021).
- [6] M. Songvilay, J. Robert, S. Petit, J. A. Rodriguez-Rivera, W. D. Ratcliff, F. Damay, V. Balédent, M. Jiménez-Ruiz, P. Lejay, E. Pachoud, A. Hadj-Azzem, V. Simonet, and C. Stock, Kitaev interactions in the Co honeycomb antiferromagnets  $\text{Na}_3\text{Co}_2\text{SbO}_6$  and  $\text{Na}_2\text{Co}_2\text{TeO}_6$ , *Phys. Rev. B* **102**, 224429 (2020).
- [7] X. Hong, M. Gillig, R. Hentrich, W. Yao, V. Kocsis, A. R. Witte, T. Schreiner, D. Baumann, N. Pérez, A. U. Wolter, Y. Li, B. Büchner, and C. Hess, Strongly scattered phonon heat transport of the candidate Kitaev material  $\text{Na}_2\text{Co}_2\text{TeO}_6$ , *Phys. Rev. B* **104**, 144426 (2021).
- [8] A. R. Wildes, V. Simonet, E. Ressouche, R. Ballou, and G. J. McIntyre, The magnetic properties and structure of the quasi-two-dimensional antiferromagnet  $\text{CoPS}_3$ , *J. Phys.: Condens. Matter* **29**, 455801 (2017).
- [9] E. Lefrançois, M. Songvilay, J. Robert, G. Nataf, E. Jordan, L. Chaix, C. V. Colin, P. Lejay, A. Hadj-Azzem, R. Ballou, and V. Simonet, Magnetic properties of the honeycomb oxide  $\text{Na}_2\text{Co}_2\text{TeO}_6$ , *Phys. Rev. B* **94**, 214416 (2016).
- [10] C. Wong, M. Avdeev, and C. D. Ling, Zig-zag magnetic ordering in honeycomb-layered  $\text{Na}_3\text{Co}_2\text{SbO}_6$ , *J. Solid State Chem.* **243**, 18 (2016).
- [11] E. A. Zvereva, M. I. Stratan, A. V. Ushakov, V. B. Nalbandyan, I. L. Shukaev, A. V. Silhanek, S. V. Streltsov, and A. N. Vasiliev, Orbitaly induced hierarchy of exchange interactions in zigzag antiferromagnetic state of honeycomb silver delafosite  $\text{Ag}_3\text{Co}_2\text{SbO}_6$ , *Dalton Trans.* **45**, 7373 (2016).
- [12] S. Eymond, M. C. Martin, and A. Durif, Donnees cristallographiques sur quelques composés isomorphes du monoarséniate de baryum-nickel:  $\text{BaNi}_2(\text{AsO}_4)_2$ , *Mater. Res. Bull.* **4**, 595 (1969).
- [13] L. Regnault, P. Burlet, and J. Rossat-Mignod, Magnetic ordering in a planar x - y model:  $\text{BaCo}_2(\text{AsO}_4)_2$ , *Phys. B+C (Amsterdam, Neth.)* **86–88**, 660 (1977).
- [14] L. Regnault, J. Boucher, J. Rossat-Mignod, J. Bouillot, R. Pynn, J. Henry, and J. Renard, Nonlinear excitations in 1D and 2D magnetic systems, *Phys. B+C (Amsterdam, Neth.)* **136**, 329 (1986).
- [15] L.-P. Regnault, C. Boullier, and J. E. Lorenzo, Polarized-neutron investigation of magnetic ordering and spin dynamics in  $\text{BaCo}_2(\text{AsO}_4)_2$  frustrated honeycomb-lattice magnet, *Heliyon* **4**, e00507 (2018).
- [16] L. Regnault and J. Rossat-Mignod, Phase transitions in quasi two-dimensional planar magnets, in *Magnetic Properties of Layered Transition Metal Compounds* (Springer, Dordrecht, 1990), pp. 271–321.
- [17] L. Regnault, C. Boullier, and J. Henry, Investigation by spherical neutron polarimetry of magnetic properties in  $\text{BaCo}_2(\text{AsO}_4)_2$ , *Phys. B (Amsterdam, Neth.)* **385–386**, 425 (2006).
- [18] R. Zhong, T. Gao, N. P. Ong, and R. J. Cava, Weak-field induced nonmagnetic state in a co-based honeycomb, *Sci. Adv.* **6**, eaay6953 (2020).
- [19] L. Y. Shi, X. M. Wang, R. D. Zhong, Z. X. Wang, T. C. Hu, S. J. Zhang, Q. M. Liu, T. Dong, F. Wang, and N. L. Wang, Magnetic excitations of the field-induced states in  $\text{BaCo}_2(\text{AsO}_4)_2$  probed by time-domain terahertz spectroscopy, *Phys. Rev. B* **104**, 144408 (2021).
- [20] X. Zhang, Y. Xu, R. Zhong, R. Cava, N. Drichko, and N. Armitage, In- and out-of-plane field induced quantum spin-

- liquid states in a more ideal Kitaev material:  $\text{BaCo}_2(\text{AsO}_4)_2$ , [arXiv:2106.13418](https://arxiv.org/abs/2106.13418).
- [21] S. Das, S. Voleti, T. Saha-Dasgupta, and A. Paramakanti, XY magnetism, Kitaev exchange, and long-range frustration in the  $J_{\text{eff}} = \frac{1}{2}$  honeycomb cobaltates, *Phys. Rev. B* **104**, 134425 (2021).
- [22] P. E. Blöchl, Projector augmented-wave method, *Phys. Rev. B* **50**, 17953 (1994).
- [23] K. Koepnik and H. Eschrig, Full-potential nonorthogonal local-orbital minimum-basis band-structure scheme, *Phys. Rev. B* **59**, 1743 (1999).
- [24] K. Riedl, Y. Li, R. Valentí, and S. M. Winter, *Ab initio* approaches for low-energy spin Hamiltonians, *Phys. Status Solidi B* **256**, 1800684 (2019).
- [25] S. M. Winter, Y. Li, H. O. Jeschke, and R. Valentí, Challenges in design of Kitaev materials: Magnetic interactions from competing energy scales, *Phys. Rev. B* **93**, 214431 (2016).
- [26] A. A. Mostofi, J. R. Yates, G. Pizzi, Y. S. Lee, I. Souza, D. Vanderbilt, and N. Marzari, An updated version of wannier90: A tool for obtaining maximally-localised Wannier functions, *Comput. Phys. Commun.* **185**, 2309 (2014).
- [27] G. Kresse and J. Furthmüller, Efficient iterative schemes for *ab initio* total-energy calculations using a plane-wave basis set, *Phys. Rev. B* **54**, 11169 (1996).
- [28] H. Eschrig, M. Richter, and I. Ophale, Relativistic solid state calculations, *Theor. Comput. Chem.* **14**, 723 (2004).
- [29] See Supplemental Material at <http://link.aps.org/supplemental/10.1103/PhysRevB.106.165131> for DFT calculation details.
- [30] G. Kresse and J. Furthmüller, Efficiency of *ab-initio* total energy calculations for metals and semiconductors using a plane-wave basis set, *Comput. Mater. Sci.* **6**, 15 (1996).
- [31] G. Kresse and J. Hafner, *Ab initio* molecular-dynamics simulation of the liquid-metal-amorphous-semiconductor transition in germanium, *Phys. Rev. B* **49**, 14251 (1994).
- [32] J. P. Perdew, K. Burke, and M. Ernzerhof, Generalized Gradient Approximation Made Simple, *Phys. Rev. Lett.* **77**, 3865 (1996).
- [33] A. I. Liechtenstein, V. I. Anisimov, and J. Zaanen, Density-functional theory and strong interactions: Orbital ordering in Mott-Hubbard insulators, *Phys. Rev. B* **52**, R5467 (1995).
- [34] H. J. Monkhorst and J. D. Pack, Special points for Brillouin-zone integrations, *Phys. Rev. B* **13**, 5188 (1976).
- [35] M. Schüler, O. E. Peil, G. J. Kraberger, R. Pordzik, M. Marsman, G. Kresse, T. O. Wehling, and M. Aichhorn, Charge self-consistent many-body corrections using optimized projected localized orbitals, *J. Phys.: Condens. Matter* **30**, 475901 (2018).
- [36] K. Koepnik, O. Janson, Y. Sun, and J. Brink, Symmetry conserving maximally projected Wannier functions, [arXiv:2111.09652](https://arxiv.org/abs/2111.09652).
- [37] K. Foyevtsova, H. O. Jeschke, I. I. Mazin, D. I. Khomskii, and R. Valentí, *Ab initio* analysis of the tight-binding parameters and magnetic interactions in  $\text{Na}_2\text{IrO}_3$ , *Phys. Rev. B* **88**, 035107 (2013).
- [38] P. Blaha, K. Schwarz, G. K. H. Madsen, D. Kvasnicka, J. Luitz, R. Laskowski, F. Tran, and L. D. Marks, *WIEN2k: An Augmented Plane Wave Plus Local Orbitals Program for Calculating Crystal Properties* (Vienna University of Technology, Vienna, 2018).
- [39] P. Blaha, K. Schwarz, F. Tran, R. Laskowski, G. K. H. Madsen, and L. D. Marks, Wien2k: An apw+lo program for calculating the properties of solids, *J. Chem. Phys.* **152**, 074101 (2020).
- [40] T. Dordević,  $\text{BaCo}_2(\text{AsO}_4)_2$ , *Acta Crystallogr., Sect. E* **64**, i58 (2008).
- [41] H. J. Xiang, E. J. Kan, S.-H. Wei, M.-H. Whangbo, and X. G. Gong, Predicting the spin-lattice order of frustrated systems from first principles, *Phys. Rev. B* **84**, 224429 (2011).
- [42] C. Wellm, W. Roscher, J. Zeisner, A. Alfonsov, R. Zhong, R. J. Cava, A. Savoyant, R. Hayn, J. van den Brink, B. Buchner, O. Janson, and V. Kataev, Frustration enhanced by Kitaev exchange in a  $\tilde{J}_{\text{eff}} = \frac{1}{2}$  triangular antiferromagnet, *Phys. Rev. B* **104**, L100420 (2021).
- [43] S. M. Winter, Magnetic couplings in edge-sharing high-spin d7 compounds, *J. Phys. Mater.* **5**, 045003 (2022).
- [44] Y. Motome, R. Sano, S. Jang, Y. Sugita, and Y. Kato, Materials design of Kitaev spin liquids beyond the Jacceli-Khaliullin mechanism, *J. Phys.: Condens. Matter* **32**, 404001 (2020).
- [45] J. G. Rau and H.-Y. Kee, Trigonal distortion in the honeycomb iridates: Proximity of zigzag and spiral phases in  $\text{Na}_2\text{IrO}_3$ , [arXiv:1408.4811](https://arxiv.org/abs/1408.4811).
- [46] J. G. Rau, E. K.-H. Lee, and H.-Y. Kee, Generic Spin Model for the Honeycomb Iridates beyond the Kitaev Limit, *Phys. Rev. Lett.* **112**, 077204 (2014).
- [47] J. Chaloupka and G. Khaliullin, Hidden symmetries of the extended Kitaev-Heisenberg model: Implications for the honeycomb-lattice iridates  $\text{A}_2\text{IrO}_3$ , *Phys. Rev. B* **92**, 024413 (2015).
- [48] T. Halloran, F. Desrochers, E. Z. Zhang, T. Chen, L. E. Chern, Z. Xu, B. Winn, M. Graves-Brook, M. Stone, A. I. Kolesnikov, Y. Qui, R. Zhong, R. Cava, Y. B. Kim, and C. Broholm, Geometrical frustration versus Kitaev interactions in  $\text{BaCo}_2(\text{AsO}_4)_2$ , [arXiv:2205.15262](https://arxiv.org/abs/2205.15262).
- [49] S. Sugano, Y. Tanabe, and H. Kamimura, *Multiplets of Transition-Metal Ions in Crystals* (Academic Press, New York, 1970).
- [50] M. Lines, Magnetic properties of  $\text{CoCl}_2$  and  $\text{NiCl}_2$ , *Phys. Rev.* **131**, 546 (1963).
- [51] S. Nishimoto, V. M. Katukuri, V. Yushankhai, H. Stoll, U. K. Röbler, L. Hozoi, I. Rousochatzakis, and J. V. D. Brink, Strongly frustrated triangular spin lattice emerging from triplet dimer formation in honeycomb  $\text{Li}_2\text{IrO}_3$ , *Nat. Commun.* **7**, 10273 (2016).
- [52] P. A. Maksimov and A. L. Chernyshev, Rethinking  $\alpha\text{-RuCl}_3$ , *Phys. Rev. Res.* **2**, 033011 (2020).
- [53] J. M. Lutinger and L. Tisza, Theory of dipole interaction in crystals, *Phys. Rev.* **70**, 954 (1946).
- [54] Y.-D. Li, X. Wang, and G. Chen, Anisotropic spin model of strong spin-orbit-coupled triangular antiferromagnets, *Phys. Rev. B* **94**, 035107 (2016).
- [55] I. Rousochatzakis, U. K. Rössler, J. van den Brink, and M. Daghofer, Kitaev anisotropy induces mesoscopic  $z_2$  vortex crystals in frustrated hexagonal antiferromagnets, *Phys. Rev. B* **93**, 104417 (2016).
- [56] P. A. Maksimov, Z. Zhu, S. R. White, and A. L. Chernyshev, Anisotropic-Exchange Magnets on a Triangular Lattice: Spin Waves, Accidental Degeneracies, and Dual Spin Liquids, *Phys. Rev. X* **9**, 021017 (2019).
- [57] E. Rastelli, A. Tassi, and L. Reatto, Non-simple magnetic order for simple Hamiltonians, *Phys. B+C (Amsterdam, Neth.)* **97**, 1 (1979).



- [58] Z. Zhu, P. A. Maksimov, S. R. White, and A. L. Chernyshev, Topography of Spin Liquids on a Triangular Lattice, *Phys. Rev. Lett.* **120**, 207203 (2018).
- [59] Z. Zhu and S. R. White, Spin liquid phase of the  $s = \frac{1}{2}J_1 - J_2$  Heisenberg model on the triangular lattice, *Phys. Rev. B* **92**, 041105(R) (2015).
- [60] P. M. C onsoli, L. Janssen, M. Vojta, and E. C. Andrade, Heisenberg-Kitaev model in a magnetic field:  $1/s$  expansion, *Phys. Rev. B* **102**, 155134 (2020).
- [61] Y. Iqbal, W.-J. Hu, R. Thomale, D. Poilblanc, and F. Becca, Spin liquid nature in the Heisenberg  $J_1 - J_2$  triangular antiferromagnet, *Phys. Rev. B* **93**, 144411 (2016).
- [62] J. B. Fouet, P. Sindzingre, and C. Lhuillier, An investigation of the quantum  $j_1$ - $j_2$ - $j_3$  model on the honeycomb lattice, *Eur. Phys. J. B* **20**, 241 (2001).
- [63] S.-S. Gong, D. N. Sheng, O. I. Motrunich, and M. P. A. Fisher, Phase diagram of the spin- $\frac{1}{2}J_1$ - $J_2$  Heisenberg model on a honeycomb lattice, *Phys. Rev. B* **88**, 165138 (2013).
- [64] S.-S. Gong, W. Zhu, D. N. Sheng, O. I. Motrunich, and M. P. A. Fisher, Plaquette Ordered Phase and Quantum Phase Diagram in the Spin- $\frac{1}{2}J_1$ - $J_2$  Square Heisenberg Model, *Phys. Rev. Lett.* **113**, 027201 (2014).
- [65] S.-S. Gong, W. Zhu, L. Balents, and D. N. Sheng, Global phase diagram of competing ordered and quantum spin-liquid phases on the kagome lattice, *Phys. Rev. B* **91**, 075112 (2015).
- [66] J. Rusna ko, D. Gotfryd, and J. Chaloupka, Kitaev-like honeycomb magnets: Global phase behavior and emergent effective models, *Phys. Rev. B* **99**, 064425 (2019).
- [67] H. Suzuki, H. Liu, J. Bertinshaw, K. Ueda, H. Kim, S. Laha, D. Weber, Z. Yang, L. Wang, H. Takahashi, K. F ursich, M. Minola, B. V. Lotsch, B. J. Kim, H. Yava , M. Daghofer, J. Chaloupka, G. Khaliullin, H. Gretarsson, and B. Keimer, Proximate ferromagnetic state in the Kitaev model material  $\alpha$ -RuCl<sub>3</sub>, *Nat. Commun.* **12**, 4512 (2021).
- [68] S. R. White, Density Matrix Formulation for Quantum Renormalization Groups, *Phys. Rev. Lett.* **69**, 2863 (1992).
- [69] M. Fishman, S. R. White, and E. M. Stoudenmire, The ITensor software library for tensor network calculations, [arXiv:2007.14822](https://arxiv.org/abs/2007.14822).
- [70] A. V. Chubukov and D. I. Golosov, Quantum theory of an antiferromagnet on a triangular lattice in a magnetic field, *J. Phys.: Condens. Matter* **3**, 69 (1991).
- [71] D. Yamamoto, G. Marmorini, and I. Danshita, Quantum Phase Diagram of the Triangular-Lattice  $XXZ$  Model in a Magnetic Field, *Phys. Rev. Lett.* **112**, 127203 (2014).
- [72] P. H. Y. Li, R. F. Bishop, and C. E. Campbell, Phase diagram of a frustrated spin- $\frac{1}{2}J_1$ - $J_2$   $XXZ$  model on the honeycomb lattice, *Phys. Rev. B* **89**, 220408(R) (2014).
- [73] C. Liu, R. Yu, and X. Wang, Semiclassical ground-state phase diagram and multi- $Q$  phase of a spin-orbit-coupled model on triangular lattice, *Phys. Rev. B* **94**, 174424 (2016).
- [74] S. Huyan, J. Schmidt, E. Gati, R. Zhong, R. J. Cava, P. C. Canfield, and S. L. Bud'ko, Hydrostatic pressure effect on the Co-based honeycomb magnet BaCo<sub>2</sub>(AsO<sub>4</sub>)<sub>2</sub>, *Phys. Rev. B* **105**, 184431 (2022).